AD_____

Award Number: DAMD17-96-1-6131

TITLE: Vascular Functional Imaging and Physiological Environment of Hyperplasia, Non-Metastatic and Metastatic Breast Cancer

PRINCIPAL INVESTIGATOR: Zaver Bhujwalla, Ph.D.

CONTRACTING ORGANIZATION: The Johns Hopkins University
Baltimore, Maryland 21205-2196

REPORT DATE: October 2000

TYPE OF REPORT: Annual

PREPARED FOR: U.S. Army Medical Research and Materiel Command
Fort Detrick, Maryland 21702-5012

1. AGENCY USE ONLY (Leave blank)	2. REPORT DATE	3. REPORT TYPE AND DATES COVERED
	October 2000	Annual (1 Oct 99 - 30 Sep 00)

4. TITLE AND SUBTITLE
Vascular Functional Imaging and Physiological Environment of Hyperplasia, Non-Metastatic and Metastatic Breast Cancer

5. FUNDING NUMBERS
DAMD17-96-1-6131

6. AUTHOR(S)
Zaver Bhujwalla, Ph.D.

7. PERFORMING ORGANIZATION NAME(S) AND ADDRESS(ES)
The Johns Hopkins University
Baltimore, Maryland 21205-2196

E-MAIL:
zaver@mri.jhu.edu

8. PERFORMING ORGANIZATION REPORT NUMBER

9. SPONSORING / MONITORING AGENCY NAME(S) AND ADDRESS(ES)
U.S. Army Medical Research and Materiel Command
Fort Detrick, Maryland 21702-5012

10. SPONSORING / MONITORING AGENCY REPORT NUMBER

11. SUPPLEMENTARY NOTES

12a. DISTRIBUTION / AVAILABILITY STATEMENT
Approved for public release; Distribution unlimited

12b. DISTRIBUTION CODE

13. ABSTRACT ***(Maximum 200 Words)***

Our goals were to understand the role of vascularization and physiological and metabolic properties in breast cancer metastasis using magnetic resonance (MR) imaging (I) and MR spectroscopy (S) of human breast cancer models.

Key findings were:

MR spectra of tumors revealed a significant differences in phospholipid composition and in intra- and extracellular pH, between control and transgene tumors formed by MDA-MB-435 human breast carcinoma cells transfected with nm23 constructs. These data demonstrate the potential of noninvasive MRS to detect forms of gene therapy which may involve transfection of cells with nm23. Choline phospholipid metabolite levels progressively increased in cultured human mammary epithelial cells (HMECs) as cells became more malignant. This work is relevant to diagnosis of breast cancer and provides a rationale for selective pharmacological intervention. Lactate levels increased significantly in cultured HMEC following malignant transformation and may promote invasive behavior and contribute to metastasis. 3-dimensional analysis of vascular volume and permeability and histological morphology demonstrated that areas of low vascular volume were associated with cell death and increasingly permeable vasculature. The more metastatic cell lines were characterized by higher vascular volume and permeability. These results indicate a potential use of MRI and MRS for evaluating 'metastatic risk' noninvasively.

14. SUBJECT TERMS	15. NUMBER OF PAGES
Research, Breast Cancer, Vascularization, Metastasis	21
	16. PRICE CODE

17. SECURITY CLASSIFICATION OF REPORT	18. SECURITY CLASSIFICATION OF THIS PAGE	19. SECURITY CLASSIFICATION OF ABSTRACT	20. LIMITATION OF ABSTRACT
Unclassified	Unclassified	Unclassified	Unlimited

NSN 7540-01-280-5500

Standard Form 298 (Rev. 2-89)
Prescribed by ANSI Std. Z39-18
298-102

TABLE OF CONTENTS

INTRODUCTION

Vascularization plays a key role in the growth and metastasis of solid tumors [1, 2]. In two recent clinical studies, breast cancer patients whose tumors had a high vascular density subsequently went on to develop metastases over a follow up period of 2.5 years [3, 4]. Statistical analyses of these patients showed that vascular density was the single most important factor ($p<0.006$) associated with subsequent formation of metastasis [4]; the other factors examined were epidermal growth factor receptor status ($p<0.01$), node status ($p<0.02$), estrogen receptor status ($p< 0.05$), tumor size ($p<0.06$), tumor grade ($p<0.5$), c-erb-2 expression ($p<0.7$), p53 ($p<0.8$) and tumor type ($p<0.8$). Studies correlating vascularization with metastasis have so far been performed with histological evaluation of excised tissue specimens as a result of which information regarding functioning of vessels is lost. Similarly, the physiological environment of these tumors, in terms of acidity and lactate production remains unknown. Thus a lack of noninvasive methods has left some vital questions about the precise nature of the relationship between vascularization and metastasis unanswered. Tumor neovascularization is induced by the secretion of angiogenic factors which act as chemotactic factors and mitogens for endothelial cells [5, 6]. One of the most potent of these is vascular endothelial growth factor (VEGF). VEGF also increases vascular permeability which in turn may allow cancer cells greater access to the vasculature [6]. In glioblastoma multiformae areas of necrosis and hypoxia show a higher expression of VEGF [7, 8]. Poorly functioning vessels and the associated hypoxia and necrosis may play a role in attracting further vascularization. Areas of hypoxia are also associated with accumulation of lactate and low pH. These two physiological factors attract neovascularization by stimulating the secretion of angiogenic factors from macrophages [9-12]. The secretion of enzymes which degrade the basement membrane in the metastatic process increases at low pH [13, 14]. Thus, vascularization, the physiological environment, and formation of metastases are highly interdependent. An understanding of the role of the physiological environment in vascularization and metastasis, and the dependence of this environment on metastatic phenotype are essential to delineate the relationship between vascularization and metastasis. Questions which are central to understanding this relationship are - (1) does the metastatic phenotype induce a higher degree of vascularization and is this mediated by modulation of the physiological environment ? (addressed in Specific Aims 1 and 3) (2) If so, do nonmetastatic tumors and preneoplastic tissue exhibit proportionately lower vascularization ? (addressed in Specific Aims 1 and 2) (3) Which particular property of the vascularization e.g. permeability, or vascular volume is the dominant factor in the dependence of metastasis on vascularization ? (addressed in Specific Aims 1 and 2) (4) Is a significant fraction of the vessels observed in the histological studies non-functional and does the resultant unsuitable environment induce expression of signals or substances which prompt and enable the cells to metastasize ? (addressed in Specific Aim 1). The overall goal of this research proposal is to use noninvasive Magnetic Resonance (MR) Imaging (I) and Spectroscopy (S) to answer the questions posed above.

BODY

The research proposed consists of three closely related aims designed to unravel the complex relationship between vascularization and metastasis. Our overall goal in this project is to determine key vascular and physiological properties which result in the close relationship between vascular density and metastasis as this information may ultimately be used to prevent tumor metastasis. We had proposed the following three aims:

Aim 1: To investigate the relationship between metastatic phenotype and the development of vascularization and evaluate the functionality of the developing vascularization in terms of vascular volume, vascular permeability and relative perfusion.
Hypothesis #1: More metastatic lines will exhibit a higher level of vascularization and permeability for similar volumes. A significant number of vessels detected by immunoperoxidase staining will not be functional and this number will increase with the size of the tumor.

Aim 2: To investigate the effect of increasing (a) tumor vascularization and (b) tumor vascularization and permeability on the formation of metastases.
Hypothesis #2: Higher vascularization and permeability will lead to an increase or an earlier incidence of metastases for all the lines.
(Aims 1 and 2 are related to questions 1-4 outlined in background)

Aim 3: To determine the relationship between metastatic phenotype and intra- and extracellular pH and lactate production.
Hypothesis #3: More metastatic lines will be more glycolytically active *in vivo*, creating an environment of high lactate and low extracellular pH for volume matched lesions.
(Aim 3 is related to question 1 outlined in background)

In the progress report for Year 1 we had presented preliminary data which demonstrated that there were significant differences in the vascular volume generated by a invasive metastatic human breast cancer line MDA-MB-231 and a nonmetastatic animal cancer line RIF-1. Studies correlating VEGF distribution with MRI maps of vascular volume and permeability demonstrated that areas around necrosis showed high expression of VEGF and were more permeable. In Year 1 we also presented data to demonstrate that there were significant differences in pH regulation and the phospholipid metabolism in solid tumors growing *in vivo* in SCID mice for a highly metastatic and a less metastatic human breast cancer line. We had therefore made significant progress in Aim 1 and Aim 3 by the end of the first year of the grant.

In Year 2 we had the following achievements. First we showed that the alterations in phospholipid metabolism observed for a highly metastatic and less metastatic tumor could be generalized to an entire panel of human mammary epithelial cells, ranging from normal to highly malignant and metastatic. We also demonstrated that lactate levels significantly increased in malignant cells compared to normal and immortalized hyperplastic human mammary epithelial cells. In addition we developed an implemented multi-slice imaging pulse sequences instead of the originally proposed single slice studies of tumors to determine the vascular characteristics over the entire tumor. In addition we developed a visualization software program which would allow us to interactively relate MRI information with histological maps.

In Year 3 used the significant technical advances made in year 2 to characterize vascular patterns for three human breast cancer lines, MDA-MB-435, MDA-MB-231 and MCF-7 inoculated in the mammary fat pad of SCID mice.

In Year 4 we have completed our comprehensive characterization of vascular patterns for three human breast cancer cell lines, MDA-MB-435, MDA-MB-231 and MCF-7 inoculated in the mammary fat pad of SCID mice. Parallel studies were performed to evaluate the invasiveness of these cells lines in an MRI based matrigel assay. VEGF levels secreted by cells and solid tumors was characterized. We also assayed the spontaneous and experimental metastastasis from these tumors models by examining lung sections stained with hematoxylin and eosin for metastatic nodules.

The technical objectives outlined in our statement of work continue to remain the same and these are: Delineate the role of vascular volume, permeability and perfusion and tumor physiological environment in the formation of metastasis from human breast cancer lines with preselected invasive and metastatic potential grown in SCID (severe combined immune deficient) mice.

EXPERIMENTAL METHODS USED FOR YEAR 4

Tumor Models and Inoculations

Human breast cancer cells were inoculated in the left upper thoracic mammary fat pad (mfp) of female severe combined immune deficient (SCID) mice. Tumor cells were inoculated in a volume of 0.05 ml Hanks balanced salt solution (HBSS, Sigma Ltd.) at a concentration of 10^6cells/0.05 ml of HBSS. Cells in culture were maintained according to previously published protocols and have similar doubling times of the order of 17-29 h. The experimental protocol was approved by the Institutional Animal Care and Use Committee. All three breast cancer lines were originally derived from pleural effusions of patients with breast cancer. Since the growth of the MCF-7 line is estrogen dependent, a 17B-Estradiol pellet (0.72 mg/pellet, 60 day release, Innovative Research of American, Sarasota, FL) was inserted in the right flank using a trochar needle, one week prior to inoculation of the cells.

Kinetics of Albumin-GdDTPA in Blood

Albumin-GdDTPA (gadolinium diethylenetriamine pentaacetic acid) was synthesized in our laboratory based on the procedure originally described by Ogan *et al.* [15]. The albumin-GdDTPA complex was dialyzed thrice against a citrate buffer and thrice against deionized water to dialyze out any free GdDTPA in the preparation. Each dialysis was performed overnight in a cold room maintained at 4°C using a dialysis membrane of MW 12-14 kd (SPECTRA/POR 4, Cole Parmer Ltd., Niles, IL). A separate set of experiments were performed to establish the kinetics of albumin-GdDTPA in blood. In these experiments, mice were anaesthetized and both the tail vein and the common carotid artery were canulated. Blood samples of 20 _l were obtained from the carotid before and up to 60 minutes after intravenous administration of albumin-GdDTPA (0.2ml of 60 mg/ml albumin-GdDTPA, Mol. Wt. ~ 90,000) delivered through the tail vein. Albumin-GdDTPA concentration in blood was obtained from the T_1 relaxation times of blood samples

measured at 4.7 T using a special micro-coil designed by V.P. Chacko (JHU), with high signal to noise ratio.
Although in this study animals were sacrificed at the end of the experiments to obtain tumors for sectioning, the availability of the micro-coil now allows us to perform repeated measurements of vascular volume and permeability on the same animal over a period of time, since blood T_1 can be determined from a couple of drops of blood obtained from the tail vein. A comparison of T_1 values from such a sample with T_1 obtained 3 minutes later from 0.5 ml of blood from the vena-cava provided almost identical values (data not shown).

Multi-slice MR Imaging Studies

Imaging studies were performed on a GE CSI 4.7 T instrument equipped with shielded gradients. Images were obtained with a 1 cm solenoid coil placed around the tumor. A small capillary filled with water doped with GdDTPA was attached to the side of the coil to (a) serve as an intensity reference, (b) ensure that spatial registration was identical for all images and, (c) reference histological sections with images. The tail vein of the animal was catheterized before it was placed in the magnet; a home-built catheter system using a small T-junction (T-Connectors, 1/16", Cole-Parmer Ltd.) was devised to minimize the dead volume, which was less than 0.04 ml. Animal body temperature was maintained at 37°C by heat generated from a pad circulating with warm water.

Multi-slice relaxation rates (T_1^{-1}) were obtained by a saturation recovery method combined with fast T_1 SNAPSHOT-FLASH imaging (flip angle of 10°, echo time of 2 ms). Images of 4-8 slices (slice thickness of 1 mm) acquired with an in-plane spatial resolution of 0.125 mm (128x128 matrix, 16mm field of view, NS=8) were obtained for 3 relaxation delays (100 ms, 500 ms, and 1s) for each of the slices. Thus T_1 maps from 8 slices could be acquired within 7 minutes. An M_0 map with a recovery delay of 7 s was acquired once at the beginning of the experiment. Images were obtained before intravenous administration of 0.2ml of 60 mg/ml albumin-GdDTPA in saline (dose of 500 mg/kg) and repeated, starting 3 minutes after the injection, up to 32 minutes. Relaxation maps were reconstructed from data sets for three different relaxation times and the M_0 data set on a pixel by pixel basis. At the end of the imaging studies, the animal was sacrificed, 0.5 ml of blood was withdrawn from the inferior vena cava, and tumors were marked for referencing to the MRI images, excised, and fixed in 10% buffered formalin for sectioning and staining. The lungs of the animal were also excised and fixed in 10% buffered formalin for sectioning and staining.

Vascular volume and permeability product surface area (PS) maps were generated from the ratio of $\Delta(1/T_1)$ values in the images to that of blood. The slope of $\Delta(1/T_1)$ ratios versus time in each pixel was used to compute PS while the intercept of the line at zero time was used to compute vascular volume [16-18]. Thus, vascular volumes were corrected for permeability of the vessels. 3-D reconstruction of MRI data was performed using our custom built volumetric visualization software. Adjustment of transfer functions that control the voxel transparency and intensity characteristics of various structures of interest can be performed with the software, to delineate structures of interest from surrounding structures. The visualization software is developed around Silicon Graphics

workstation systems, taking full advantage of the hardware accelerated graphics capabilities such as 2- and 3D textures to provide interactive rendering results. Furthermore, by displaying the image for each parameter through a unique color channel e.g. vascular volume as red and vascular permeability as green, it is feasible to visually inspect the relationship between two parameters by fusing the two color maps.

Analysis of MRI Tumor Vascular Characteristics

In addition to deriving average vascular volume and permeability over the entire tumor, we separately analyzed regions of high vascular volume or high vascular permeability using a selected threshold for the highest 10% or 25% of the distribution. One reason for this approach is that the original histological observations relating vessel density to disposition to metastasize was obtained by counting the number of vessels in the regions of high vascular density [3]. The other reason was to investigate the relationship between vascular volume and vascular permeability in regions of high vascular volume and regions of high vascular permeability. For our analyses, we therefore determined mean values of vascular volume in regions of high vascular volume as well as high permeability. Similar analyses were performed for permeability. In addition, the percent fractional tumor volume containing high vascular volume or high vascular permeability was also determined. 3D volume data were processed with an operator independent computer program which enabled selection, mapping and display of the regions within a specified range of parameter values. Volume fractions of the regions were determined using the histogram analysis of the volume data. The routine is written with IDL programming language (Research Systems, Boulder, CO) and is compatible with most operation systems.

Statistical Methods

Four to eight tumors were studied for each group. All tumors were volume matched with volumes of 200-300 mm^3. Statistical analyses were performed using Statview II version 1.04, 1991 (Abacus Concepts, Inc., Berkeley, CA). Statistically significant differences were established using a two-sided unpaired t-test for 95% confidence levels or higher ($P<0.05$).

Histological Analysis of Tumors

Adjacent 5 μm thick histological sections obtained at 500 μm intervals through the tumor were stained with hematoxylin and eosin. Sections were digitized with a CCD camera (Sanyo Ltd., CA) attached to an optical microscope.

Assays for Spontaneous and Experimental Metastasis

Spontaneous metastasis from the cell lines was evaluated by determining the size and number of nodules in the lungs of animals sacrificed following MRI. Nodules were identified by microscopic examination of at least three 5 μm thick lung sections stained with hematoxylin and eosin.
A separate assay was performed to evaluate experimental metastasis from these cell lines. For this assay, 2×10^6 cells were injected into the tail vein in a volume of 0.05 ml HBSS. Five animals were

used for each cell line. The animals were sacrificed two weeks later and lung sections were examined as described before.

Assays for VEGF expression for Cells used in the Study

Quantitation of VEGF in Conditioned Media of Breast Cancer: VEGF was measured by the Quantikine (R&D Systems Inc., MN) enzyme-linked immunosorbent assay. 10^6 cells were seeded in a 100 mm petri dish overnight. Conditioned media from each of the cell lines were collected, centrifuged and diluted as per manufacturer's instructions prior to performing the assay. The assay was repeated thrice using duplicate samples each time.

MRI Invasion Assays to determine invasive characteristics of the cell lines used in this study

A comparison of the invasive behavior of the cell lines used in this study was performed using our MR compatible invasion assay system. A detailed description of the assay can be found in Pilatus *et al.* [19]. Briefly, the assay system consists of a layer of reconstituted basement membrane, Matrigel® (Sigma, St. Louis, MO), sandwiched between cells. The system is perfused under well controlled conditions of temperature and oxygenation. The assay is stable over a period of at least three days and allows dynamic measurements of invasion over this time. In the study here, the assay was used to confirm previously established observations regarding the invasiveness of the cell lines studied.

RESULTS

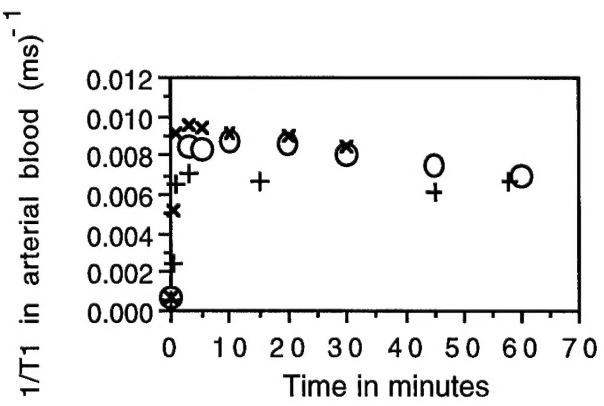

Figure 1: Kinetics of albumin-GdDTPA in mouse blood for normal mouse (+), mouse with MDA-MB-231 tumor (o) and mouse with DU-145 tumor (x). Blood levels of albumin-GdDTPA remain constant up to 30 minutes and longer. The lower $1/T_1$ in (+) is due to initial loss of blood during canulation of the carotid for this animal.

The kinetics of albumin-GdDTPA over a period of time for one normal and two tumor bearing animals are shown in Figure 1. These data confirm previous observations that the concentration of albumin-GdDTPA remains constant in the vasculature up to at least 30 minutes [20]. Representative histological sections stained with hematoxylin and eosin together with lung sections demonstrating metastatic nodules for the respective tumor are shown in Figure 2(A-F). The arrows mark blood vessels in the histological sections which typically consist of a single layer of endothelial cells. Data of vascular volume and permeability for the three tumor models are summarized in Table 1(A) and 1(B). Volumetric analyses were performed for the highest 10% and 25% histogram values of vascular volume and permeability as well as mean vascular volume and permeability for size matched tumors. For the panel of breast tumor models, MDA-MB-435 demonstrated significantly higher vascular volume compared to MDA-MB-231 and MCF-7 tumors for the highest 10% and 25% analyses.

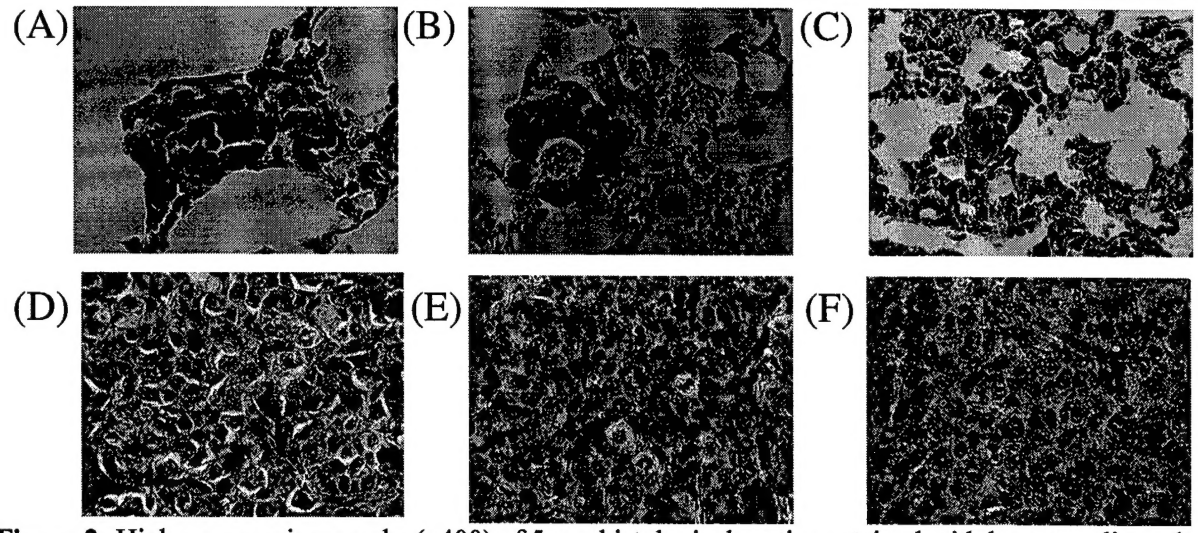

Figure 2: High-power micrographs (x400) of 5 µm histological sections stained with hematoxylin and eosin. Sections D, E and F are primary tumor sections obtained from MDA-MB-435, MDA-MB-231and MCF-7 tumors. Arrow indicates tumor vessels. Sections A, B and C are lung sections demonstrating metastasis of MDA-MB-435 (spontaneous metastasis), MDA-MB-231 (spontaneous metastasis), MCF-7 (experimental metastasis) cancer cells.

Both MDA-MB-435 and MDA-MB-231 breast tumor models were significantly more permeable in terms of mean values than MCF-7 tumors for the highest 10% and 25% analyses. In addition, volumetrically, MDA-MB-231 tumors were also significantly more permeable than MCF-7 tumors.

Table 1A: Vascular volume data summarized for the three tumor models

Cancer Model	Tumor Volume in mm^3	Highest 10% values of histogram		Highest 25% values of histogram		All non-zero values of histogram	
Breast		% Volume	Mean value in µl/g	% Volume	Mean value in µl/g	% Volume	Mean value in µl/g
MDA-MB-435 (n=8)	212± 31	8.2± 0.4	67.7±12.4#	20.4±0.9	45.6±7.0#	81.3±3.6	18.4±3.1
MDA-MB-231 (n=4)	287± 62	8.6± 0.4	36.8±5.2	21.3±1.0	27.2±3.7	85.1±3.8	11.0±2.7
MCF-7 (n=6)	270 ± 44	8.8±0.5	32.7±4.8	22.1± 1.2	24.5±3.4	88.1± 4.9	12.5± 2.5

Values are Mean ± 1 S.E.M.; n represents the number of tumors studied per model with at least four to six slices per tumor. # significantly different from MCF-7;

Table 1B: Permeability data summarized for the three tumor models

Cancer Model	Tumor Volume in mm^3	Highest 10% values of Histogram		Highest 25% values of Histogram		All non-zero values of Histogram	
Breast		% Volume	Mean value in µl/g-min	% Volume	Mean value in µl/g-min	% Volume	Mean value in µl/g-min
MDA-MB-435 (n=8)	212± 31	7.5± 0.8	4.2± 0.6#	19.0± 2.1	2.6± 0.3#	74.6± 8.2	0.91± 0.1#
MDA-MB-231 (n=4)	287± 62	9.2± 0.2#	3.5± 1.1#	23.0± 0.5#	2.4± 0.7#	91.3± 1.8#	1.24± 0.4#
MCF-7 (n=6)	270 ± 44	7.6± 0.6	1.5± 0.3	19.0± 1.5	1.1± 0.2	75.4± 6.1	0.5± 0.1

Values are Mean ± 1 S.E.M.; n represents the number of tumors studied per model with at least four to six slices per tumor. # significantly different from MCF-7.

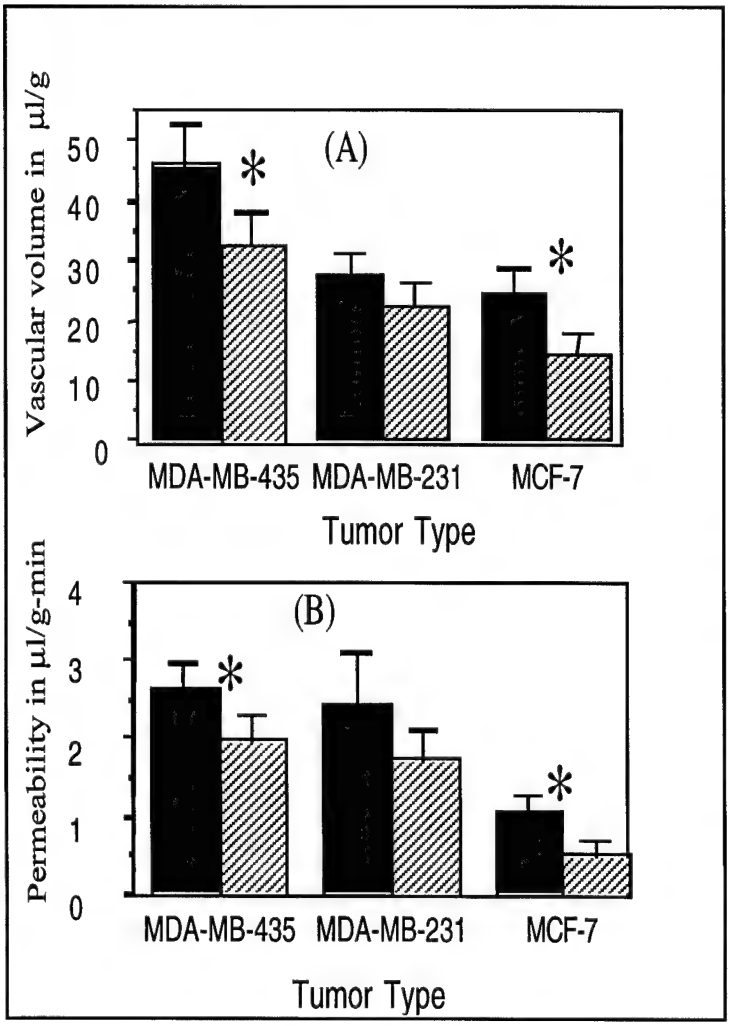

Figure 3: Vascular volume and permeability 'mismatch' characteristics of breast and prostate cancer tumor models. The mean value of the highest 25% values of vascular volume (solid bars), and the mean vascular volumes spatially corresponding to the highest 25% values of permeability (hatched bars) are shown in Figure 3(A). The mean value of the highest 25% of permeability values (solid bars), and the permeability spatially corresponding to the highest 25% values of vascular volume (hatched bars) are shown in Figure 3(B). A significant difference ($P<0.05$) was observed for all the tumor models. The only exception to this was for the MDA-MB-231 tumor group.

Another facet of vasculature, revealed from these analyses, was that regions of high vascular volume were not spatially coincident with regions of high permeability. A significant difference was observed for all the tumor models (Figure 3). The only exception to this was observed for the MDA-MB-231 tumor group. When three larger tumors of approximately 500-600 mm^3 volume, which were excluded from the size matched data, were added to the MDA-MB-231 group, the mismatch for the vascular volume was significant but

there was still no significant difference in permeability (Figure 3). Analyses of VEGF expression for the cell lines are presented in Table 2. MDA-MB-231 cells secreted the highest levels of VEGF, followed by MDA-MB-435 cells. MCF-7 cells secreted the lowest amount of VEGF.

Results from the assays of spontaneous and experimental metastasis are presented in Table 3. MDA-MB-435 and MDA-MB-231 tumors exhibited spontaneous . MCF-7 tumors did not result in the formation of spontaneous metastasis. While all three cell lines were capable of forming experimental lung metastasis, again as for the spontaneous metastasis assay, MCF-7 cells induced the fewest lung nodules.

Table 2: VEGF secretion by cell lines

Tumor Model	VEGF^{+} in pg/10^6 cells (in culture)
Breast cancer	
MDA-MB-435	161.8 ± 9.8
MDA-MB-231	422.7 ± 156
MCF-7	66.5 ± 5.0

$^{+}$Values for ELISA assay represent Mean ± 1 S.E.M.

While our cancer cell lines were preselected for literature established differences in invasive characteristics, the phenotypic characteristics of cell lines can vary amongst laboratories. We therefore performed studies to confirm the invasion patterns of the cell lines. These data are presented in Figure 4.

From these images it is apparent that the Matrigel layer is significantly degraded by MDA-MB-435 and MDA-MB-231 cells, while in comparison MCF-7 cells do not degrade the Matrigel layer. The mean invasion index ± 1 S.E.M. for n separate experiments at approximately 47 h for the six cell lines was as follows: MDA-MB-435, 2.65 at 49 h, n=1; MDA-MB-231, 1.4 ± 0.3 at 49.1 h, n=2; MCF-7, 0.04 ± 0.1 at 49.3 h, n=2. These data demonstrate that, as anticipated, MDA-MB-435 and MDA-MB-231 cells were invasive and MCF-7 exhibited hardly any invasiveness for this assay.

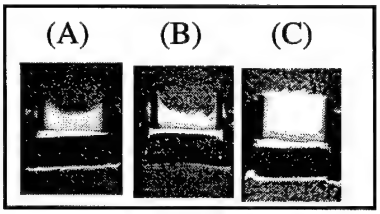

Figure 4 (A-C): 'Metabolic Boyden Chamber Assay' demonstrating differences in invasive characteristics of the breast (A-C) cell lines at approximately 47 h. The T_1 weighted ^{1}H MR images show the bright Matrigel layer which is significantly degraded by (A) MDA-MB-435, and (B) MDA-MB-231 but not by the (C) MCF-7 cells.

Table 3: Assays of Spontaneous and Experimental Metastasis for the tumor models used in the study.

Tumor Model	Spontaneous Metastasis$^{\xi}$ (number of animals with lung nodules/total number of animals studied)	Experimental Metastasis$^{\chi}$ (number of animals with lung nodules/total number of animals studied)
MDA-MB-435	4/9	6/7
MDA-MB-231	2/7	4/6
MCF-7	0/8	1/7

$^{\xi}$Average time from inoculation of cancer cells to excision of tumor and lungs was approximately 5 weeks for the breast cancer . $^{\chi}$Lungs excised 2 weeks after injecting 10^6 cells in the tail vein.

DISCUSSION

Vascular volume and permeability measurements

Accurate quantitation of vascular volume and vascular permeability using the algorithm described in this study requires the assumption that the concentration of contrast agent in the blood remains constant over the time period of MRI data acquisition which was validated here. The second assumption is that water in the vascular and extravascular compartments is in fast-exchange. Data from isolated rat heart perfusion studies suggest that water exchange may be intermediate in the heart [21, 22]. However, rat cardiac vessel walls are well organized and consist of smooth muscle cell lining as well as a layer of basement membrane which may result in some restriction of water exchanging across the two compartments. In contrast, as demonstrated in our results, tumor neovasculature typically consists of a single layer of endothelial cells which facilitates fast exchange. Further validation of this assumption comes from studies by van Dijke et al. [23] where a highly significant correlation of the order of 0.9 was observed between vessel density and MRI derived values of vascular volume. Because of the noninvasive nature of MRI the technique is able to measure vascular volume corrected for permeability. With invasive techniques some leakage of the tracer will occur in highly permeable regions as soon as the tracer enters the circulation, which might lead to overestimation of values [24]. However, while measurements of vascular volume and permeability for the six tumor models used here have not been performed previously using either MRI or other techniques, the values of vascular volume and permeability obtained here are in reasonably good agreement with values for other solid tumors cited in literature obtained with traditional invasive methods [16, 24-26].

Relationship between Vascular Volume and Permeability, and Necrosis

A comparison of histological sections obtained from the imaged tumors consistently showed that areas of cell death and necrosis were typically associated with low or non-detectable vascular volume, although areas of low vascular volume were not always associated with necrosis in histological sections. Some vessels in large necrotic areas were found to contain clumps of tumor cells. These vessels were surrounded by dead cells suggesting this as one of the mechanisms for vascular collapse in highly metastatic tumors.

We also consistently observed that regions with high vascular volume were significantly less permeable when compared with regions of high permeability within the same tumor. Similarly regions of high permeability consistently exhibited lower vascular volumes. One explanation for these observations is that regions of low vascular volume are the most hypoxic and therefore will express higher VEGF. This is consistent with previous observations that more intense VEGF staining is detected around areas of necrosis [7, 8, 27] where the vessels are also most permeable [17, 28]. Another possible mechanism for the 'mismatch' is the occurrence of lymphatic drainage which is currently under investigation in our laboratory. These findings do imply that in addition to previously proposed mechanisms of high tumor interstitial pressure [29, 30] the delivery of macromolecular agents to the tumor interstitium may also be limited by the lower permeability of tumor vasculature in precisely those viable vascular areas where they necessarily should be delivered for effective treatment.

Vascular Characteristics and VEGF expression

The patterns of VEGF expression obtained for the cell lines were in agreement with previously published values of VEGF levels for MCF-7 and MDA-MB-231 cells [31]. Not surprisingly, rather than vascular volume, VEGF expression by the cells was most closely related to the permeability measured in the solid tumors. The two cell lines with the lowest expression of VEGF, MCF-7, displayed low permeability while the cell lines with higher expression of VEGF, MDA-MB-231 and MDA-MB-435 exhibited higher permeability. MDA-MB-231 was also the only tumor model where the permeability in regions of high vascular volume was not significantly different from regions of low vascular volume.

Invasion, Metastasis and Vascularization

These experiments were designed to determine the vascular characteristics of breast and prostate cancer models preselected for differences in invasive and metastatic behavior. To determine the ability of MRI to predict the disposition of the tumor to metastasize, the experimental protocol would have required excising the tumor and allowing the animal to survive surgery and determining the metastasis in lungs and other organs at time of natural death. To justify such a protocol an initial study was required to demonstrate significant differences between vascular characteristics of the selected tumor models as is demonstrated here. In the framework of this study we established that within the breast and prostate tumor model groups, tumor models which demonstrated the ability to establish pulmonary metastases to the lung from primary tumors consistently showed significantly higher permeability and, with the exception of MDA-MB-231, higher vascular volume. These data are consistent with results from Melnyk *et al.* [32], where inhibition of VEGF was found to prevent tumor dissemination by a mechanism which may be distinct from its effect on tumor growth.

The metastatic characteristics of the two breast lines MDA-MB-435 and MDA-MB-231 and the non-metastatic characteristic of MCF-7 cells are consistent with previous observations [33, 34]. Results from studies with poorly invasive MCF-7 cells transfected to overexpress the angiogenic factor FGF-1 demonstrate that angiogenic capability alone does not determine the metastatic end-point [35]. Thus, cancer cells expressing both high invasive and angiogenic capacity represent the most lethal phenotype.

KEY RESEARCH ACCOMPLISHMENTS:

The major findings to emerge from the research studies performed thus far are :

• NMR spectra of primary tumors in SCID mice revealed a dramatic and consistent difference in the phospholipid composition of control and transgene tumors formed by derivatives of MDA-MB-435 human breast carcinoma cells transfected with nm23 constructs. Significant differences in intra and extracellular pH were also detected for solid tumors derived from these lines. This was one of the first *in vivo* observations to link the activity of a putative metastasis suppressor gene to metabolic processes. The data also demonstrate the potential of noninvasive NMR spectroscopy to detect forms of gene therapy which may involve transfection of cells with nm23.

• Choline phospholipid metabolite levels progressively increased in cultured HMEC as cells become more malignant. We therefore propose that carcinogenesis in human breast epithelial cells results in progressive alteration of membrane choline phospholipid metabolism. This work is relevant to diagnosis of breast cancer and also provides a rationale for selective pharmacological intervention.

• Lactate levels increase significantly in cultured HMEC following malignant transformation. However, following malignant transformation, there did not appear to be a close dependence between lactate levels observed in malignant cell lines and the metastatic potential of these lines. The increased lactate production may result in an acidic environment which may promote invasive behavior and contribute to metastasis.

• 3-dimensional interactive analysis of vascular volume and permeability and histological morphology demonstrates that areas of low vascular volume are associated with cell death and increasingly permeable vasculature. Regions of high vascular volume and high vascular permeability do not coincide spatially. These findings imply that in addition to previously proposed mechanisms of high tumor interstitial pressure, the delivery of macromolecular agents to the tumor interstitium may also be limited by the lower permeability of tumor vasculature in precisely those viable vascular areas where they necessarily should be delivered for effective treatment.

• The more metastatic cell lines are characterized by higher vascular volume and vascular permeability *in vivo* for analysis performed for regions of high vascular volume and permeability. Cancer cells expressing both high invasive and angiogenic capacity represent the most lethal phenotype. The results indicate a potential use of MRI for evaluating 'metastatic risk' noninvasively.

CONCLUSIONS

The results obtained demonstrate that there are significant differences in vascular characteristics between the metastatic and non or less metastatic lines. High vascular volume and high vascular permeability characterized the most metastatic breast cancer line. The non metastatic human breast cancer line MCF-7 exhibited a lower vascular volume as well as lower vascular permeability. Results from studies with poorly invasive MCF-7 cells transfected to overexpress the angiogenic factor FGF-1 demonstrate that angiogenic capability alone does not determine the metastatic end-point [35]. Thus, cancer cells expressing both high invasive and angiogenic capacity represent the most lethal phenotype.

It is essential to characterize the vasculature of the regions of high vascular volume or permeability, since the significance is less apparent when averaging the measurements over the entire tumor. This demonstrates the necessity of techniques which can detect vascular characteristics with spatial information.

Regions of high vascular volume and high vascular permeability do not coincide spatially within the same tumor. Regions of low vascular volume were usually associated with foci of necrosis in the histological sections. High permeability was related to a higher expression of VEGF. These findings imply that in addition to previously proposed mechanisms of high tumor interstitial pressure [29, 30] the delivery of macromolecular agents to the tumor interstitium may also be limited by the lower permeability of tumor vasculature in precisely those viable vascular areas where they necessarily should be delivered for effective treatment.

We are currently performing studies related to investigating the effects of increasing tumor vascularization and tumor vascularization and permeability on the formation of metastases.

REPORTABLE OUTCOMES

Peer reviewed manuscripts

1. Aboagye, E. and Bhujwalla, Z. M. Malignant Transformation Alters Membrane Phospholipid Metabolism of Human Mammary Epithelial Cells. *Cancer Research,* 59, 80-84, 1999.

2. van Sluis R, Bhujwalla Z, Raghunand N, Ballesteros P, Alvarez J. Cerdan S Gillies RJ. Imaging of extracellular pH of tumors using 1H MRSI. *Magnetic Resonance in Medicine,* 41: 743-750, 1999.

3. Bhujwalla, Z. M., Aboagye, E. O., Gillies, R. J., Chacko, V. P., Mendola, C. E., Backer, J. M. Nm23-transfected MDA-MB-435 human breast carcinoma cells form tumors with altered phospholipid metabolism and pH. A ^{31}P NMR study *In vivo* and *In vitro. Magnetic Resonance in Medicine,* 41: 897-903, 1999 .

4. Aboagye, E., Artemov, D., Senter, P. D. and Bhujwalla, Z. M. Intratumoral Conversion of 5-Fluorocytosine to 5-Fluorouracil by Monoclonal Antibody-Cytosine Deaminase Conjugates: Noninvasive detection of prodrug activation by Magnetic Resonance Spectroscopy and Spectroscopic Imaging. *Cancer Research,* 58, 4075-4078, 1998.

5. Ravi, R., Mookerjee, B., Bhujwalla, Z. M., Hayes Sutter, C., Artemov, D., Zeng, Q., Dillehay, L. E., Madan, A., Semenza, G. L. and Bedi, A. Regulation of tumor angiogenesis by p53-induced degradation of hypoxia-inducible factor 1α. *Genes and Development*, 14(1): 34-44, 2000.

6. Aboagye, E. O, Mori, N. and Bhujwalla, Z. M. Effect of Malignant Transformation on Lactate Levels of Human Mammary Epithelial Cells, *Advances in Enzyme Regulation*, (in press), 2000.

Review article

7. Gillies, R. J., Bhujwalla, Z. M., Evelhoch, J., Garwood, M., Neeman, M., Robinson, S. P., Sotak, C. H., van der Sanden, B. Applications of Magnetic Resonance in Model Systems I: Tumor Biology and Physiology. *Neoplasia,* 2(1):1-14, 2000.

Invited Review

8. Bhujwalla, Z. M., Artemov, D., Glockner, J. Tumor angiogenesis, vascularization and contrast enhanced MRI. *Topics in Magnetic Resonance Imaging,* 10(2):92-103, 1999.

9. Bhujwalla, Z. M., Artemov, D., Solaiyappan, M. Insights into Tumor Vascularization using Magnetic Resonance Imaging and Spectroscopy. *Experimental Oncology*, Vol. 22, pp 3-7, 2000.

Symposium Proceedings

10. Bhujwalla, Z. M., Artemov, D., Aboagye, E., Ackerstaff, E., Gillies, R. J., Natarajan, K., Solaiyappan, M. The Physiological Environment in Cancer Vascularization, Invasion and Metastasis. *Novartis Foundation Symposium Proceedings* (in press), 2000.

Published abstracts from presentations at conferences (listed for 2000 only)

11. Bhujwalla, Z. M., Artemov, D. A., Solaiyappan, M.. Vascular characterization of human breast cancer and prostate cancer models. *Proceedings of the Eigth Scientific Meeting of the ISMRM*, Denver, 2000.

Funding awarded based on work supported by this award

NIH (Bhujwalla, Z.M., P.I.) 07/01/99-06/30/04
1 R01 CA82337-01
'Hostile Environments Promote Invasion and Metastasis'
The aim of these studies is to identify the interaction between the physiological environment and inflammatory signaling and vascularization in breast cancer invasion and metastasis and the ability of anti-inflammatory agents to prevent invasion and metastasis.

NIH (Bhujwalla, Z. M., P.I.) 03/01/00-02/28/03
1 P20 CA86346

'Multidisciplinary Functional Imaging of Cancer'
This application was funded to establish a 'Pre-In vivo Cellular and Molecular Imaging Center'

REFERENCES

1. Folkman J. How is blood vessel growth regulated in normal and neoplastic tissue ? Cancer Research 1986; 46: 467-473.

2. Liotta LA, Steeg PS, Stetler-Stevenson WG. Cancer metastases and angiogenesis: an imbalance of positive and negative regulation. Cell 1991; 64: 327-336.

3. Weidner N, Semple JP, Welch WR, Folkman J. Tumor angiogenesis and metastasis--correlation in invasive breast carcinoma. N Engl J Med 1991; 324: 1-8.

4. Horak ER, Leek R, Klenk N, LeJeune S, Smith K, Stuart N, Greenall M, Stepniewska K, Harris AL. Angiogenesis, assessed by platelet/endothelial cell adhesion molecule antibodies, as indicator of node metastases and survival in breast cancer. Lancet 1992; 340: 1120-4.

5. Folkman J, Merler, E., Abernathy, C., Williams, G. Isolation of a tumor factor responsible for angiogenesis. J. Exp. Med. 1971; 133: 275-288.

6. Moses MA, The role of vascularization in tumor metastasis, *in* "Microcirculation in cancer metastasis", F. William Orr, Buchanan, M.R., Weiss, L., Eds. 1991, CRC Press: p. 257-276.

7. Shweiki D, Itin A, Soffer D, Keshet E. Vascular endothelial growth factor induced by hypoxia may mediate hypoxia-initiated angiogenesis. Nature 1992; 359: 843-5.

8. Plate KH, Breier G, Weich HA, Risau W. Vascular endothelial growth factor is a potential tumour angiogenesis factor in human gliomas in vivo. Nature 1992; 359: 845-8.

9. Cooper RG, Taylor CM, Choo JJ, Weiss JB. Elevated endothelial-cell stimulating angiogenic factor activity in rodent glycolytic skeletal muscles. Clinical Science 1991; 81: 267-270.

10. Knighton DR, Hunt TK, Scheuenstuhl H, Banda M. Oxygen tension regulates the expression of angiogenesis factor by macrophages. Science 1983; 221: 1283-1285.

11. Knighton D, Schumerth S, Fiegel V, Environmental regulation of macrophage angiogenesis., *in* "Current Communications in Molecular Biology, Angiogenesis: Mechanisms in Pathobiology.", D.B. Rifkin, Klagsbrun, M., Eds. 1987, Cold Spring Harbor Laboratory: p. 150-157.

12. Jensen AJ, Hunt B, Scheuenstuhl B, Banda MJ. Effect of lactate, pyruvate and pH on secretion of angiogenesis and mitogenesis factors by macrophages. Laboratory Investigations 1986; 56: 574-578.

13. Rozhin J, Sameni M, Ziegler G, Sloane BF. Pericellular pH affects distribution and secretion of Cathepsin B in Malignant cells. Cancer Research 1994; 54: 6517-6525.

14. Kato Y, Nakayama Y, Umeda M, Miyazaka K. Induction of 103kDa gelatinase/type IV collagenase by acidic culture conditions in mouse metastatic melanoma cell lines. J. Biol. Chem. 1992; 267: 11424-11430.

15. Ogan MD, Schmiedl U, Moseley ME, Grodd W, Paajanen H, Brasch RC. Albumin labeled with Gd-DTPA. An intravascular contrast-enhancing agent for magnetic resonance blood pool imaging: preparation and characterization [published erratum appears in Invest Radiol 1988 Dec;23(12):961]. Invest Radiol 1987; 22: 665-71.

16. Braunschweiger PG, Schiffer LM. Effect of dexamethasone on vascular function in RIF-1 tumors. Cancer Res 1986; 46: 3299-303.

17. Bhujwalla ZM, Artemov D, Glockner J. Tumor angiogenesis, vascularization, and contrast-enhanced magnetic resonance imaging. Top Magn Reson Imaging 1999; 10: 92-103.

18. Ravi R, Mookerjee B, Bhujwalla ZM, Sutter CH, Artemov D, Zeng Q, Dillehay LE, Madan A, Semenza GL, Bedi A. Regulation of tumor angiogenesis by p53-induced degradation of hypoxia-inducible factor 1alpha. Genes Dev 2000; 14: 34-44.

19. Pilatus U, Ackerstaff E, Artemov D, Mori N, Gillies RJ, Bhujwalla ZM. Imaging prostate cancer invasion with multi-nuclear magnetic resonance methods: the Metabolic Boyden Chamber. Neoplasia 2000; 2: 273-9.

20. Schmiedl U, Ogan M, Paajanen H, Marotti M, Crooks LE, Brito AC, Brasch RC. Albumin labeled with Gd-DTPA as an intravascular, blood pool-enhancing agent for MR imaging: biodistribution and imaging studies. Radiology 1987; 162: 205-10.

21. Donahue KM, Burstein D, Manning WJ, Gray ML. Studies of Gd-DTPA relaxivity and proton exchange rates in tissue. Magn Reson Med 1994; 32: 66-76.

22. Donahue KM, Weisskoff RM, Parmelee DJ, Callahan RJ, Wilkinson RA, Mandeville JB, Rosen BR. Dynamic Gd-DTPA enhanced MRI measurement of tissue cell volume fraction. Magn Reson Med 1995; 34: 423-32.

23. van Dijke CF, Brasch RC, Roberts TP, Weidner N, Mathur A, Shames DM, Mann JS, Demsar F, Lang P, Schwickert HC. Mammary carcinoma model: correlation of macromolecular contrast- enhanced MR imaging characterizations of tumor microvasculature and histologic capillary density. Radiology 1996; 198: 813-8.

24. Tozer GM, Morris CC. Blood flow and blood volume in a transplanted rat fibrosarcoma: comparison with various normal tissues. Radiother Oncol 1990; 17: 153-65.

25. Peterson H-I, Vascular and extravascular spaces in tumors: tumor vascular permeability., *in* "Tumor Blood Circulation: Angiogenesis, vascular morphology and blood flow of experimental and human tumors.", H.-I. Peterson, Eds. 1979, CRC Press: Boca Raton. p. 77-85.

26. Sands H, Shah SA, Gallagher BM. Vascular volume and permeability of human and murine tumors grown in athymic mice. Cancer Lett 1985; 27: 15-21.

27. Shweiki D, Neeman M, Itin A, Keshet E. Induction of vascular endothelial growth factor expression by hypoxia and by glucose deficiency in multicell spheroids: implications for tumor angiogenesis. Proc Natl Acad Sci U S A 1995; 92: 768-72.

28. Furman-Haran E, Margalit R, Grobgeld D, Degani H. Dynamic contrast-enhanced magnetic resonance imaging reveals stress- induced angiogenesis in MCF7 human breast tumors. Proc Natl Acad Sci U S A 1996; 93: 6247-51.

29. Jain RK. Transport of molecules across tumor vasculature. Cancer and Mestastasis Reviews 1987; 6: 559-593.

30. Jain RK. Transport of molecules in the tumor interstitium: a review. Cancer Res 1987; 47: 3039-51.

31. Hyder SM, Murthy L, Stancel GM. Progestin regulation of vascular endothelial growth factor in human breast cancer cells. Cancer Res 1998; 58: 392-5.

32. Melnyk O, Shuman MA, Kim KJ. Vascular endothelial growth factor promotes tumor dissemination by a mechanism distinct from its effect on primary tumor growth. Cancer Res 1996; 56: 921-4.

33. Price JE, Polyzos A, Zhang RD, Daniels LM. Tumorigenicity and metastasis of human breast carcinoma cell lines in nude mice. Cancer Res 1990; 50: 717-21.

34. Thompson EW, Brunner N, Torri J, Johnson MD, Boulay V, Wright A, Lippman ME, Steeg PS, Clarke R. The invasive and metastatic properties of hormone-independent but hormone-responsive variants of MCF-7 human breast cancer cells. Clin Exp Metastasis 1993; 11: 15-26.

35. Zhang L, Kharbanda S, McLeskey SW, Kern FG. Overexpression of fibroblast growth factor 1 in MCF-7 breast cancer cells facilitates tumor cell dissemination but does not support the development of macrometastases in the lungs or lymph nodes. Cancer Res 1999; 59: 5023-9.